Progress in Additive Manufacturing (2023) 8:693–701
https://doi.org/10.1007/s40964-023-00418-7

FULL RESEARCH ARTICLE

# The influence of printing parameters on the mechanical properties of 3D printed TPU-based elastomers

V. M. Bruère[1] · A. Lion[1] · J. Holtmannspötter[2] · M. Johlitz[1]

Received: 7 September 2022 / Accepted: 19 February 2023 / Published online: 2 March 2023


**Abstract**
Additive Manufacturing (AM) becomes more and more focus of studies in the scientific community. Nevertheless, elastomers in 3D printing are still a relatively understudied topic despite their extensive use in machine components. The further understanding of the technologies and knowledge acquirement are fundamental steps towards the improvement of the printing process and the broadening of feasible applications of 3D printed elastomers. This work focused on thermoplastic polyurethanes printed with Fused Filament Fabrication (FFF) and investigated the effect of infill deposition angle and contour lines on the tensile and the stress relaxation behaviour. Samples were printed in alternating as well as unidirectional infill orientations, the latter without and with outlines. Tensile tests revealed that alternating orientations of 0°–90° and 45°–135° have a similar behaviour and benefit the integrity of the part. The fully unidirectional orientation at 90° hindered the tensile strength due to the absence of outlines and consequent delamination. All comparative analyses displayed a low influence of the raster angle at lower strains. Stress relaxation results showed similar behaviour for samples with outlines, without a clear effect of the infill orientations. In summary, contour lines are essential and an alternating orientation is recommended for better part integrity.

**Keywords** Thermoplastic polyurethanes · Fused filament fabrication · Infill deposition angle · Contour lines

## 1 Introduction

Additive Manufacturing (AM) is increasingly causing an impact on today's manufacturing scenarios. The ease of on-demand fabrication of complex parts on site, with reduced waste and post-processing, as well as no need for individual tooling [1–4] are among AM's main advantages. Furthermore, the constant development of new technologies and materials substantially facilitates a deeper immersion of 3D printing in the market.

In the prototyping field, AM particularly benefits the Research & Development by producing components faster than with conventional methods. This saves costs and allows more time for further investigations. 3D printed parts may enable better assessments of design and mechanical performance, identification of errors in early stages and improvements in subsequent numerical analysis for conceptual design optimisation. A work from Goularte et al. [5] took advantage of 3D printing to produce and test four types of AM soft polymers, assisting in their material characterization. Numerical simulations with a commercial finite-element software enabled a design optimisation of aircraft seal profiles.

Polymers represent a majority in AM. Despite that, 3D printed polymer parts are usually not able to provide a mechanical performance comparable to traditional fabrication [6, 7], hindering their further exploration in technical applications. In the scope of elastomers, components such as seals, hoses and membranes age during operation and often need replacement. This leads to significant warehousing costs and logistics challenges. Therefore, the adoption of AM is of great value. Generally, the conventional elastomers cannot be used in the current AM technologies, as vulcanization is not easily transferred into the processes. Each 3D printer is designed to a certain type and nature of material. Requirements include liquid, filament or powder

✉ V. M. Bruère
vivianne.bruere@unibw.de

[1] Institute of Mechanics, University of the Bundeswehr Munich, Neubiberg, Germany

[2] Bundeswehr Research Institute for Materials, Fuels and Lubricants, Erding, Germany

form, and the material should be a thermoplastic, UV-cured resin or silicone.

Particularly for Fused Filament Fabrication (FFF), the partial melting of a material extruded through a heated nozzle is required. Hence, for the printing of soft polymers, thermoplastic elastomers are employed, being thermoplastic polyurethanes (TPU) frequently used. They exhibit an ease of stretching and bending, as a result of the physical crosslinks between soft segments based on polyester/polyether chains and hard segments based on isocyanates [8]. Printing with TPUs on FFF machines is a challenging task. The low stiffness of the filaments induces buckling and hinders the extrusion control [9], which is intensified the softer the material. Moreover, they are sensitive to moisture. This impairs both the final quality of the parts and the extrusion process, sometimes leading to the interruption of the print jobs [10]. The influence of liquid media on printed geometries and their resulting mechanical behaviour was investigated in Loos et al. [11]. Bruère et al. [12] examined the under-extrusion related to the feeding system and caused by moisture absorption by the filament prior to printing. Other works in the literature explored the 3D printing of soft polymers. Tayeb et al. [13] studied the residual strain, softening and hysteresis of a thermoplastic styrenic elastomer under cyclic loading, while Leon-Calero et al. [14] focused on the chemical composition, thermal behaviour and damping capacity in compression for a range of commercial TPUs.

In spite of that, works on AM of elastomers are still modest compared to other materials. Therefore, intense research is required, targeting on the understanding of elastic polymers mechanical behaviour associated with the printing parameters. In this regard, this paper evaluates the influence of infill orientations and perimeter lines on the quasi-static mechanical behaviour, as well as on the viscoelastic properties of a commercial TPU printed in FFF. First, a comparative analysis of the microstructure and the tensile properties of samples with alternating oriented infill was carried out. The study continued with the mechanical characterization of samples with unidirectional rasters. Afterwards, the combination of contour lines and unidirectional infill was analysed regarding both the uniaxial tensile and the stress relaxation behaviour.

## 2 Materials and methods

Print jobs were performed on an Ultimaker S5 printer equipped with a Bowden extruder (filament diameter of 2.85 mm and nozzle diameter of 0.4 mm). All specimens were printed flat on the build plate (horizontal build orientation). The printing parameters were adapted from the manufacturer's suggestions combined with print trial experiences. Mainly, lower printing speeds were used, which are fundamental for the reduction of buckling and under-extrusion when printing with soft filaments.

Tensile and relaxation tests were carried out to study the quasi-static and rate-dependent behaviour of a polyether polyurethane [11] TPU filament from the company Recreus (Spain), called Filaflex 70A (hardness of 70 Shore A), with a glass transition within the negative temperature range of − 70 °C to − 50 °C [14]. The tensile tests were performed on a ZwickRoell universal testing machine with a force sensor of 500 N at ambient temperature for a total of 5 specimens per sample. The displacement rates were of 0.63 mm/s for Part A and 0.25 mm/s for Part B and Part C. The relaxation tests were performed on the same machine and conditions for samples stretched with an initial rate of 3 mm/s up to a 70% elongation for a duration of 6 h. In this case, three specimens were tested to verify the repeatability of the results, and one of them is presented and discussed.

### 2.1 Part A

At first, a comparison with a work from Xiao and Gao [15] was carried out. Dumbbell specimens were directly printed one at a time. Two alternating raster orientations relative to the tensile direction between the individual layers were obtained: 0°–90° and 45°–135°. Both types contained two contour lines and similar dimensions to Xiao and Gao [15]. They were taken from the ISO 37 Type 2 Standard, considering the same thickness of 1.1 mm used by the authors. The printing parameters are listed in Table 1. For hygroscopic reasons, the filament was pre-dried at 50 °C for 6 h.

Only one printing temperature was investigated, as this was the temperature that provided better extrusion from preliminary tests and experience. Moreover, since Xiao and Gao [15] used a different material (a medical grade TPU Tecoflex LM-95A from Lubrizol—USA), no comparative quantitative analysis was performed. The focus was on the reproduction of similar printings to qualitatively compare the quasi-static behaviour of the samples and to obtain an indication of the alternating raster orientation that provided the best results.

**Table 1** Printing parameters for samples from Part A

| Parameters | Quantity |
|---|---|
| Printing temperature (°C) | 240 |
| Bed temperature (°C) | – |
| Printing speed (mm/s) | 10 |
| Layer thickness (mm) | 0.38 |
| Layer height (mm) | 0.3 (1st) \| 0.2 |
| Contour lines (–) | 2 |
| Flow (%) | 106 |
| Infill percentage (%) | 100 |

### 2.2 Part B

In a second stage, the tensile strength of a unidirectional raster orientation was investigated for angles of 0°, 45° and 90°. Plates of $60 \times 60 \times 2$ mm$^3$ were printed and punched into dumbbell geometries according to the DIN 53504 S3A Standard. This enabled a uniform cross section transition while ensuring the unidirectional orientation without the need of contour lines and avoiding a stepwise transition, which would affect the tests. The printing parameters are seen in Table 2. When signs of moisture absorption were detected, the filament was dried at 50 °C for 4–6 h.

### 2.3 Part C

In the third part of the study, dumbbell specimens were directly printed with dimensions according to the DIN 53504 S3A Standard. Unidirectional rasters at 0° or 90° were applied, along with two contour lines for uniform transition of the geometry. Due to hygroscopic properties, the filaments were dried for 6 h at 50 °C and stored in a box with humidity control while printing. Table 3 contains the printing parameters. The mechanical testing for this part concentrated on both tensile and relaxation tests.

For the relaxation results, a curve fitting to the experimental data in the Python programming language was performed. The objective was to analyse the viscoelastic parameters and predict the equilibrium stress for the stress relaxation. To this end, a generalized Maxwell viscoelasticity model (Eq. 1) was considered and evaluated. The expression for the time-dependent stress was rewritten with the help of Eq. (2). Then, the stress $\sigma(t)$ was expressed as a function of the Maxwell element parameters and the maximum stress $\sigma_0$ for the fitting, as Eq. (3) shows. The parameters $\sigma_i$ and $\tau_i$ are, respectively, the stress-like constant and relaxation time for the $i$th Maxwell element.

$$\sigma(t) = \sigma_{eq} + \sum_{i=1}^{n} \sigma_i \exp\left(-\frac{t}{\tau_i}\right), \tag{1}$$

**Table 2** Printing parameters for samples from Part B

| Parameters | Quantity |
|---|---|
| Printing temperature (°C) | 240 |
| Bed temperature (°C) | – |
| Printing speed (mm/s) | 15 |
| Layer thickness (mm) | 0.38 |
| Layer height (mm) | 0.27 (1st) \| 0.1 |
| Contour lines (–) | – |
| Flow (%) | 106 |
| Infill percentage (%) | 100 |

**Table 3** Printing parameters for samples from Part C

| Parameters | Quantity |
|---|---|
| Printing temperature (°C) | 240 |
| Bed temperature (°C) | – |
| Printing speed (mm/s) | 10 |
| Layer thickness (mm) | 0.38 |
| Layer height (mm) | 0.15 (1st) \| 0.2 |
| Contour lines (–) | 2 |
| Flow (%) | 110 (1st) \| 106 |
| Infill percentage (%) | 100 |

$$\sigma_{eq} = \sigma(t=0) - \sum_{i=1}^{n} \sigma_i \exp\left(-\frac{0}{\tau_i}\right) = \sigma_0 - \sum_{i=1}^{n} \sigma_i, \tag{2}$$

$$\sigma(t) = \sigma_0 - \sum_{i=1}^{n} \sigma_i \left[1 - \exp\left(-\frac{t}{\tau_i}\right)\right]. \tag{3}$$

## 3 Results and discussion

### 3.1 Part A

Figure 1 shows the microstructure of the samples after failure. The strain of the 90° layers in the specimen with a 0°–90° infill orientation is visible through the sinusoidal lines, distancing themselves from each other. For the 45°–135° oriented specimen, the lines were distorted into the tensile loading direction. The tensile test results are in Table 4, with the stress–strain curves in Fig. 2.

The microstructures were analogous to those in Xiao and Gao's work [15], as well as the comparative results between

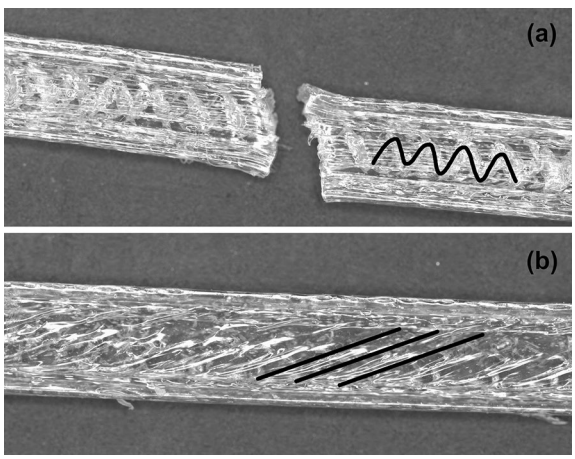


**Fig. 1** Top view of specimens from samples **a** A1 and **b** A2 after the tensile test

**Table 4** Tensile properties for samples from Part A

| Sample | Raster angle (°) | Maximum stress (MPa) | Strain at break (%) | Young's modulus at 50% strain (MPa) |
|---|---|---|---|---|
| A1 | 0°–90° | 11.06 ± 0.92 | 808.95 | 4.69 |
| A2 | 45°–135° | 12.01 ± 0.56 | 895.68 | 4.36 |
| A3 | 0°–90° | 12.44 ± 0.37 | 822.33 | 4.67 |

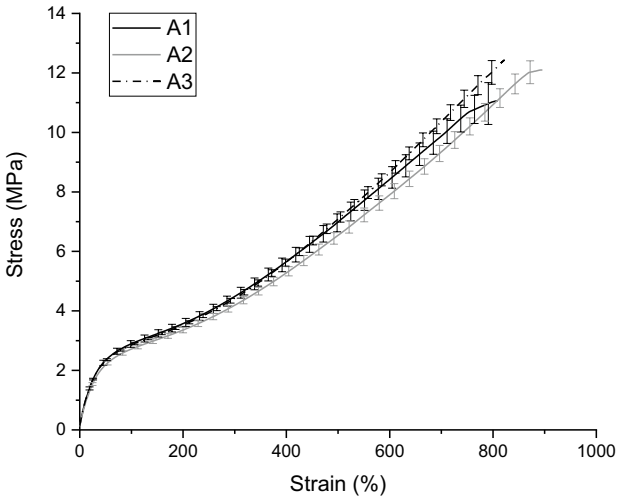


**Fig. 2** Tensile stress–strain curves from Part A

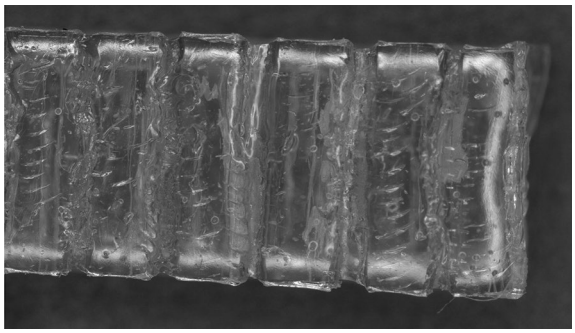

**Fig. 3** Top view of specimen from sample B1 after the tensile test

the two grid orientations. All samples obtained high elongations at break and similar ultimate stress values. Samples A1 and A2 had a respective percentage deviation of 11% and 3.5% with respect to sample A3. The greater differences in the strengths between samples A1 and A3 with the same infill orientation is noteworthy. This is a consequence of the Bowden extruder, which is more prone to buckling and compromised extrusion of soft filaments than the Direct Drive [12]. The results show the impact of the feeding system on the printing reproducibility of elastic materials, confirming the variability of the process. Furthermore, the Young's modulus at 50% strain was verified. Although the tensile strengths of samples A1 and A3 had some deviation, their elastic moduli were apart by less than 0.5%. This indicates the great similarity in their behaviour and the minor impact of the process variability in the lower strain range. Sample A2 presented the lowest Young's modulus, approx. 7% lower than A1 and A3.

Although the reproducibility was somewhat compromised, the ultimate stresses are similar and do not vary much (standard deviations below 10%). Samples A1 and A2 presented the greater deviations among the individual specimens, interfering on the average values. Nevertheless, for both alternating infill orientations, the curve shapes were alike, with scarcely any influence at lower strain levels. Up to 400% strain, samples A1 and A3 had the same stiffness, while A2 achieved a slightly lower stress. It can be stated that, under lower deformations, the orientation of the alternating infill has no effective influence on the tensile strength of the part. However, it must be pointed out that the degree alternation between the subsequent layers directly affects the sample integrity. This can be visualised in Fig. 1a. The 90° lines tended to separate due to the perpendicular loading direction, but the 0°-layer underneath helped in keeping these lines together and avoiding a premature failure.

## 3.2 Part B

The microstructure of the failure for a sample B1 specimen is seen in Fig. 3. For this specific case, the great impact of the absence of contour lines for the unidirectionally oriented, punched specimen can be observed. Both contour lines and a previous layer shifted by 90° relative to the current layer would have better maintained the integrity of the samples had they been present. TPUs exhibit a great layer-to-layer adhesion [16]. For semi-crystalline polymers such as PEEK, surface crystallization between printed layers takes place, leading to poor weld strength [17]. However, DSC investigations (not included in this contribution) showed a mostly amorphous behaviour, with no crystallization peaks even for varying cooling rates, and no apparent melting, i.e., low crystallinity content. Hence, the likely reduced interfacial crystallinity did not degrade much the interlayer bond strength. The separation of the perpendicular lines within

**Table 5** Tensile properties for samples from Part B

| Sample | Raster angle (°) | Maximum stress (MPa) | Strain at break (%) | Young's modulus at 50% strain (MPa) |
|---|---|---|---|---|
| B1 | 90° | 9.75 ± 0.19 | 1139.65 | 4.19 |
| B2 | 0° | 14.73 ± 0.26 | 1387.45 | 3.93 |
| B3 | 45° | 14.87 ± 0.46 | 1492.38 | 3.77 |

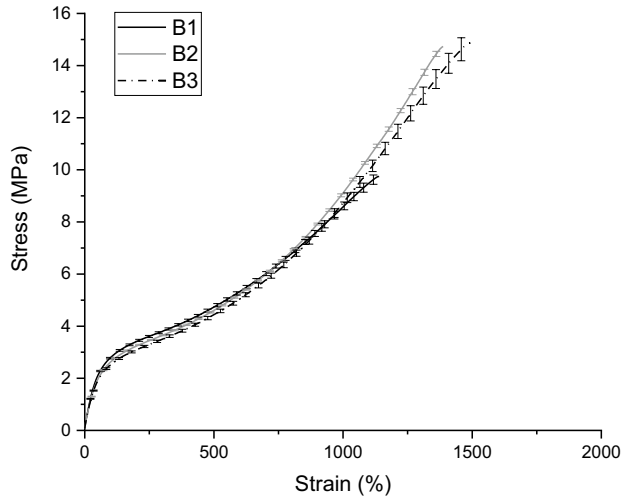


**Fig. 4** Tensile stress–strain curves from Part B

the same layer due to the tensile loading was the dominant cause for a premature failure.

Table 5 gathers the tensile test results, also seen in the stress–strain curves in Fig. 4. Indeed, the 90° orientation provided the lowest ultimate stress, approx. 33.8% and 34.4% lower than the 0° and 45° samples, respectively. Nevertheless, all samples reached high elongations at break, displaying values above 1000%. The results are in line with findings reported in the literature. The 90° infill parts exhibit lower tensile strengths, and their failure relies upon the adhesion between adjacent rasters. With the application of the loading perpendicular to the raster orientation, the intralayer bond suffers delamination, as the stress concentrates in this narrow region [18–21].

Samples oriented at 0° and 45° presented similar results, with deviations in the ultimate stresses lower than 1% from one another. The 45° sample stiffness was constantly somewhat lower than for the 0° sample. Similar to Part A, all three curves had the same shape and no significant differences in the lower strain range (less noticeable below 100%). In fact, the elastic moduli at 50% strain were in a similar range for all infill orientations. The greatest difference was of less than 10% for sample B1 relative to sample B3. It can be affirmed that the unidirectional infill orientations at 0° and 45° do not have a considerable influence on the tensile strength of the parts. The 90° orientation, however, is critical and should be attentively considered the greater the applied deformation is.

**Table 6** Tensile properties for samples from Part C

| Sample | Raster angle (°) | Maximum stress (MPa) | Strain at break (%) | Young's modulus at 50% strain (MPa) |
|---|---|---|---|---|
| C1 | 90° | 15.17 ± 0.46 | 1303.96 | 4.53 |
| C2 | 0° | 14.48 ± 0.83 | 1215.94 | 4.65 |

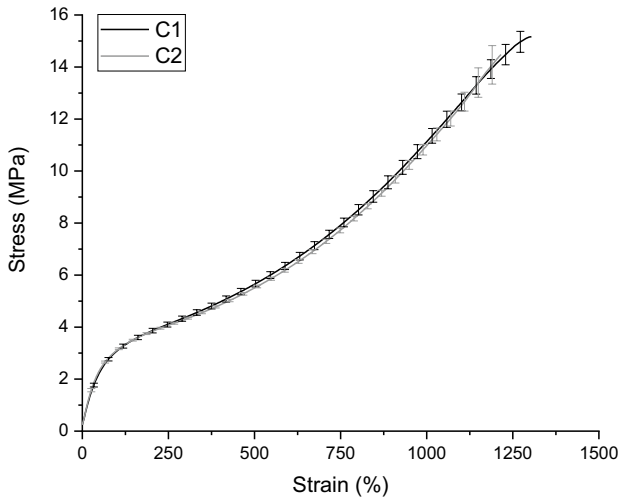


**Fig. 5** Tensile stress–strain curves from Part C

## 3.3 Part C

The tensile tests for the unidirectionally oriented samples with two contour lines showed different results in comparison to Part B. From Table 6 and Fig. 5, the influence of perimeter lines in the sample is evident, as the 90° infill sample achieved a higher ultimate stress than before.

Sample C1 reached similar values to sample C2, whose tensile strengths deviated in less than 5% from one another. In this case, the sample oriented at 90° had the contour lines as connection points for the infill. With the tensile loading, the perpendicular infill lines within the same layer

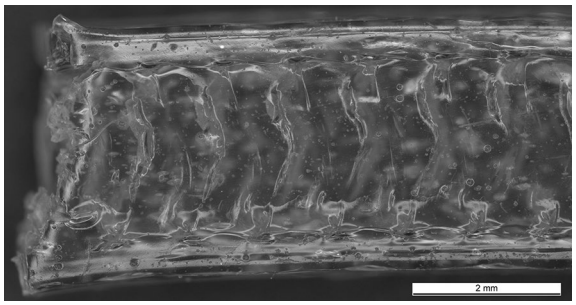


**Fig. 6** Top view of specimen from sample C1 after the tensile test

were prevented from an easy detachment and consequent delamination. The sample maintained its integrity for greater stresses and, unlike sample B1, avoided a premature failure. This is illustrated in Fig. 6, where the microstructure of sample C1 after failure showed a good adhesion between the infill and the perimeters and significantly less line separation than in Fig. 3. There is a lack of works in the literature regarding the influence of the presence/absence of contours in a geometry. Some studies, however, investigated the number of contour lines and reported the positive effect on the tensile strength with the increase of outlines. The resistance of the part is improved due to the addition of longitudinal filaments in the loading direction [22, 23], which assists in carrying the load [20].

Samples C1 and C2 displayed the same curve shape and stiffness. At 50% strain, for instance, their Young's modulus distanced themselves in approx. 2.6%. It was concluded that the addition of perimeters diminishes the influence of unidirectional infill orientations at the considered angles. Once again, high deformations beyond 1000% were obtained. A likely explanation for the slightly lower tensile strength of sample C2 is related to the printing process itself. As previously discussed, the Bowden-driven printer offers less extrusion control for elastic filaments. This may have randomly induced more flaws (or closer flaws) in the material flow for sample C2. A fracture mechanics approach could corroborate this statement. Furthermore, the printing temperature should be sufficiently high to promote a proper welding interface [20, 24, 25]. The bonding process is thermally driven, and cooling between rasters leads to partial bonding [26]. As the geometries from Part C were directly printed, the infill path at 90° travels less than the path at 0° and allows less cooling time between adjacent deposited rasters, as reported by Ai and Vogt [27]. Hence, the intralayer welding, and consequently the tensile strength, of sample C1 may have also been affected by the shorter cooling time.

Among the tensile experiments, it was noted that Part B samples exhibited the lowest elastic moduli. This can be justified by the printing speed, which was higher than for Part A and C. As mentioned, this parameter is particularly relevant in elastic filaments due to the increased tendency to under-extrusion. Moreover, it is known in the literature that higher printing speeds have a negative effect on the stiffness and tensile strength. This was verified in a meta-analysis performed by Farashi and Vafaee [28]. The authors related the deposition speed to the heating and cooling cycles, affecting the temperature gradient, which is the major factor for the bonding of the layers.

The geometric differences between Part A and Part B and C also influenced the results. The ultimate elongation varies linearly with the ratio of the squared root of the initial cross-sectional area to the initial gauge length, i.e., $\sqrt{A_0}/L_0$ [29]. This explains the lower strain at break values for Part A samples, since their thickness was lower and their gauge length was larger than for Part B and C. Another fact observed in all samples from all parts is plasticity after the tensile tests. For samples C1 and C2, the plastic deformation was around 33%, with thickness and width ratios (between values after and before the test) varying from 0.74 to 0.79. This is an important factor to consider for applications with 3D printed parts with a TPU filament in FFF machines.

Small air gaps could be particularly noted in Figs. 3 and 6. Extrusion failures as such when printing with elastic filaments are difficult to avoid. They induce cracks in the geometry and may affect the tensile strength to some degree, although minor considering their size. Furthermore, it is worth mentioning that the effect of the layer height is not so significant [20], as this study considered a horizontal building orientation. When printed vertically, the layer height has a greater influence on the part, since the bonding between the layers would be subjected to separation by the perpendicular loading application, leading to lower tensile strengths [19, 21, 25, 30, 31].

In the relaxation tests, the samples reached similar maximum stress levels. Table 7 gathers the information regarding infill orientation and maximum stress for the studied samples C3 and C4.

Both samples did not exhibit a clear equilibrium stress $\sigma_{eq}$ in the experiments. Several optimisation runs were performed to find the viscoelastic parameters, and a total of seven Maxwell elements provided the best results. Tables 8 and 9 show the fitted parameters and the resulting equilibrium stresses. At least one relaxation time per time decade was obtained, which is recommended for a proper

**Table 7** Maximum stresses from stress relaxation for samples from Part C

| Sample | Raster angle (°) | Maximum stress (MPa) |
|---|---|---|
| C3 | 90° | 2.55 |
| C4 | 0° | 2.51 |

**Table 8** Elastic ($\sigma_{eq}$ [MPa]) and viscoelastic ($\sigma_i$ [MPa], $\tau_i$ [s]) parameters from the curve fitting for sample C3

| $\sigma_{eq}$ | $\sigma_1$ | $\sigma_2$ | $\sigma_3$ | $\sigma_4$ | $\sigma_5$ | $\sigma_6$ | $\sigma_7$ |
|---|---|---|---|---|---|---|---|
| 1.2008 | 2.2041E − 1 | 2.1702E − 1 | 1.7374E − 1 | 1.5040E − 1 | 1.3814E − 1 | 1.4809E − 1 | 3.0423E − 1 |
| – | $\tau_1$ | $\tau_2$ | $\tau_3$ | $\tau_4$ | $\tau_5$ | $\tau_6$ | $\tau_7$ |
| – | 7.4891E − 1 | 6.1968 | 3.4833E1 | 1.6724E2 | 7.9488E2 | 3.6820E3 | 4.1608E4 |

**Table 9** Elastic ($\sigma_{eq}$ [MPa]) and viscoelastic ($\sigma_i$ [MPa], $\tau_i$ [s]) parameters from the curve fitting for sample C4

| $\sigma_{eq}$ | $\sigma_1$ | $\sigma_2$ | $\sigma_3$ | $\sigma_4$ | $\sigma_5$ | $\sigma_6$ | $\sigma_7$ |
|---|---|---|---|---|---|---|---|
| 1.2956 | 1.9363E − 1 | 1.9223E − 1 | 1.7156E − 1 | 1.3664E − 1 | 1.3623E − 1 | 1.6015E − 1 | 2.2584E − 1 |
| – | $\tau_1$ | $\tau_2$ | $\tau_3$ | $\tau_4$ | $\tau_5$ | $\tau_6$ | $\tau_7$ |
| – | 6.3774E − 1 | 4.4436 1 | 2.2482E1 | 1.0076E2 | 4.1258E2 | 2.1018E3 | 1.7016E4 |

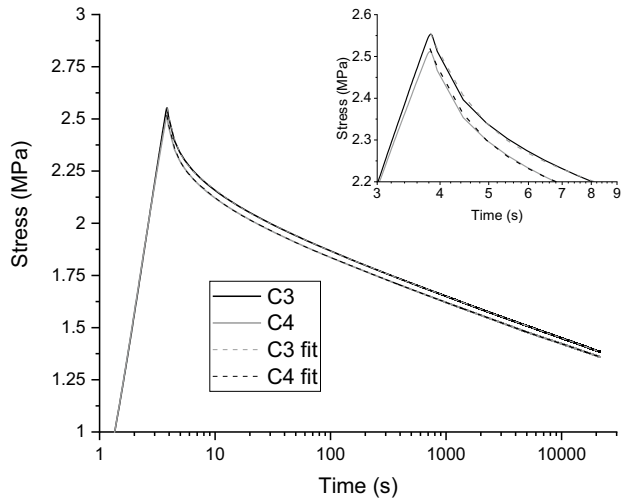


**Fig. 7** Stress relaxation curves from Part C

representation of the relaxation behaviour. The resulting viscoelastic parameters for C3 and C4 are similar in order of magnitude. Both fittings presented one relaxation time per time decade from $10^{-1}$ to $10^4$ s, except for the $10^2$ s-time decade with two relaxation times. All stress-like constants of the Maxwell elements were between 0.1 and 0.3 MPa, denoting the similarity of their elastic components. The R-squared values for the fittings were 0.999991 and 0.999996 for C3 and C4, respectively, demonstrating the suitability of the optimisation.

Figure 7 shows the plotting over time in a semi-logarithmic scale of the experimental data for both samples with their respective fitted curves. A similar relaxation behaviour of C3 and C4 can be observed, as well as the visual quality of the fitting. The equilibrium stress was not reached in the total duration of the tests. Despite that, the last recorded stress for C4 is away from the equilibrium in less than a 5% deviation, according to the fitted viscoelastic model. For sample C4, the equilibrium is to be met in almost 2 days of stress relaxation. For C3, however, the model predicted a total of 6 days to face a deviation of ~ 15% of the last recorded stress to the equilibrium.

Half of the total stress relaxation occurred at 92 s and 52 s for C3 and C4, respectively. This shows the rapidity of the relaxation within the first minutes. Sample C4 relaxed slightly faster than C3, both in the experiments and in the viscoelastic model. Hence, the chain mobility of sample C4 appears to be somewhat higher. A likely explanation is the print deposition path. The infill lines oriented at 90° were distorted into the tensile direction during loading, as discussed in the Part A analysis. This may restrict the reorientation of the components within the material to adjust the applied stress in comparison to the infill oriented at 0° (C4), since the stress relaxation depends on the capacity of the polymer chains to rearrange themselves under the application of a load [32]. Costanzo et al. [33] measured the molecular orientation for PLA printed samples and identified that the polymer chains become oriented in the flow direction. In addition, the authors stated that the flow-induced deformation of the filament surface cannot fully relax due to higher shear and cooling rates. Nonetheless, this lack of relaxation is related to the insufficient time for this phenomenon and consequent entrapment of orientation at glass transition. As TPUs generally have low glass transition temperatures (in fact, negative values for Filaflex 70A), the welding occurs

away from the glass transition. Furthermore, the samples were printed at low speeds. This leads to slower cooling and, consequently, lower temperature gradients, inferring that the polymer chains were relaxed before testing.

Moreover, C4 presented stress values lower than C3 throughout the course of the relaxation. Nevertheless, the difference in the stresses between the samples remained low and practically the same since the maximum stress. Sample C4 constantly showed a deviation of around 1.6–1.8% from sample C3. Analogous to C1 and C2 tensile results, this can be justified by the printing process variability. Therefore, no precise statement on the influence of the infill angle can be made regarding the relaxation behaviour. Future studies are recommended to investigate the chain mobility of the prints from a microscopic point of view and to verify if the printing strategy affects the relaxation performance.

## 4 Conclusions

The influence of infill deposition angle and contour lines on the tensile and relaxation behaviour of an elastic TPU filament printed on FFF was carried out. The investigation was divided into three parts.

Part A evaluated the microstructure of alternatively oriented infills, exhibiting the distortion of the infill lines into the tensile loading direction. The impact of the printer feeding system on sample reproducibility was verified, since the Bowden extruder is more prone to buckling and a compromised extrusion. Moreover, the infill direction alternation had an important role in keeping the integrity of the print.

In Part B, the tensile tests of the unidirectionally oriented infill samples revealed the major influence of the absence of contour lines on the integrity of the print and its strength, particularly for the 90° sample. For both Part A and B, the differences in the tensile behaviour of the varied orientations were relevant for the higher strain range.

For Part C, the addition of outlines indicated to neutralize the effect of infill orientation in the tensile strength. The main advantage is the connection points for the 90° infill and the drastic reduction of layer delamination. The viscoelastic parameters for the stress relaxation curves obtained by optimisation runs presented analogous results for the Maxwell element stresses, denoting the similarity of the elastic components of both infill orientations. Although the 0° infill suggests a faster stress relaxation than the 90°, the low deviation between the stresses may be a consequence of the printing process variability. Therefore, no influence of the infill orientation could be surely affirmed for the employed printing parameters.

Finally, all tensile tests displayed high elongation at break despite considerable residual deformation. The minor influence of the infill orientation on the lower strain range of the stress–strain curves and the beneficial addition of contour lines are a valuable information for the production of parts for technical applications. Due to the amount of printing parameters in FFF and large variation on print quality, additional studies (e.g., the number of outlines) are advisable for a thorough optimisation of the printing process with elastic filaments. Future investigations on a microscopic level are also recommended for a chain mobility analysis for improved material characterization. At last, the results can be generalized to other TPU filaments, given the similar nature of the materials. However, the same cannot be assured for non-elastic materials.

**Acknowledgements** This research is funded by dtec.bw—Digitalization and Technology Research Center of the Bundeswehr, which we gratefully acknowledge dtec.bw is funded by the European Union—NextGenerationEU.

**Funding** Open Access funding enabled and organized by Projekt DEAL.

**Data availability** The authors confirm that the data supporting the findings of this study are available within the article.

## Declarations

**Conflict of interest** On behalf of all authors, the corresponding author states that there is no conflict of interest.



## References

1. Klahn C, Leutenecker B, Meboldt M (2015) Design strategies for the process of additive manufacturing. Proc CIRP 36:230–235
2. Janusziewicz R, Tumbleston JR, Quintanilla AL et al (2016) Layerless fabrication with continuous liquid interface production. P Natl Acad Sci USA 113(42):11703–11708
3. Ford S, Despeisse M (2016) Additive manufacturing and sustainability: an exploratory study of the advantages and challenges. J Clean Prod 137:1573–1587
4. Bikas H, Stavropoulos P, Chryssolouris G (2016) Additive manufacturing methods and modelling approaches: a critical review. Int J Adv Manuf Tech 83:389–405
5. Goularte BF, Bruère VM, Lion A et al (2023) Multiparametric optimisation of 3D printed aircraft door seals. Proceedings of the munich symposium on lightweight design. Springer Vieweg, Berlin

6. Lukić M, Clarke J, Tuck C et al (2016) Printability of elastomer latex for additive manufacturing or 3D printing. J Appl Polym Sci. https://doi.org/10.1002/app.42931
7. Ligon SC, Liska R, Stampfl J et al (2017) Polymers for 3D printing and customized additive manufacturing. Chem Rev 117(15):10212–10290
8. Drobny JG (2014) Handbook of thermoplastic elastomers. Elsevier, Amsterdam
9. Gilmer EL, Miller D, Chatham CA et al (2018) Model analysis of feedstock behavior in fused filament fabrication: enabling rapid materials screening. Polymer 152:51–61
10. Herzberger J, Sirrine JM, Williams CB et al (2019) Polymer design for 3D printing elastomers: recent advances in structure, properties, and printing. Prog Polym Sci 97:101144
11. Loos K, Bruère VM, Demmel B et al (2021) Future-oriented experimental characterization of 3D printed and conventional elastomers based on their swelling behavior. Polymers 13:4402
12. Bruère VM, Lion A, Holtmannspötter J et al (2022) Under-extrusion challenges for elastic filaments: the influence of moisture on additive manufacturing. Prog Addit Manuf. https://doi.org/10.1007/s40964-022-00300-y
13. Tayeb A, Le Cam JB, Loez B (2022) 3D printing of soft thermoplastic elastomers: effect of the deposit angle on mechanical and thermo-mechanical properties. Mech Mater 165:104155
14. León-Calero M, Reyburn Valés SC, Marcos-Fernández Á et al (2021) 3D printing of thermoplastic elastomers: role of the chemical composition and printing parameters in the production of parts with controlled energy absorption and damping capacity. Polymers 13:3551
15. Xiao J, Gao Y (2017) The manufacture of 3D printing of medical grade TPU. Prog Addit Manuf 2(3):117–123
16. Gregor-Svetec D (2022) Polymers in printing filaments. In: Izdebska-Podsiadly J (ed) Polymers for 3D printing. William Andrew Publishing, Norwich, pp 155–269
17. Collinson DW, von Windheim N, Gall K et al (2022) Direct evidence of interfacial crystallization preventing weld formation during fused filament fabrication of poly (ether ether ketone). Addit Manuf 51:102604
18. Rajpurohit SR, Dave HK (2018) Effect of process parameters on tensile strength of FDM printed PLA part. Rapid Prototyping J 24(8):1317–1324
19. Hanon MM, Marczis R, Zsidai L (2019) Anisotropy evaluation of different raster directions, spatial orientations, and fill percentage of 3D printed PETG tensile test specimens. Key Eng Mater 821:167–173
20. Bakir AA, Neshani R, Özerinç S (2021) Mechanical properties of 3D-printed elastomers produced by fused deposition modeling. Fused deposition modeling based 3D printing. Springer International Publishing, Cham, pp 107–130
21. Hanon MM, Dobos J, Zsidai L (2021) The influence of 3D printing process parameters on the mechanical performance of PLA polymer and its correlation with hardness. Procedia Manuf 54:244–249
22. Mahmood S, Qureshi AJ, Goh KL et al (2017) Tensile strength of partially filled FFF printed parts: meta modelling. Rapid Prototyping J 23(3):524–533
23. Gebisa AW, Lemu HG (2019) Influence of 3D printing FDM process parameters on tensile property of ULTEM 9085. Procedia Manuf 30:331–338
24. Coogan TJ, Kazmer DO (2020) Prediction of interlayer strength in material extrusion additive manufacturing. Addit Manuf 35:101368
25. Fang L, Yan Y, Agarwal O et al (2020) Processing-structure-property relationships of bisphenol-A-polycarbonate samples prepared by fused filament fabrication. Addit Manuf 35:101285
26. Fitzharris ER, Watt I, Rosen DW et al (2018) Interlayer bonding improvement of material extrusion parts with polyphenylene sulfide using the Taguchi method. Addit Manuf 24:287–297
27. Ai JR, Vogt BD (2022) Size and print path effects on mechanical properties of material extrusion 3D printed plastics. Prog Addit Manuf 7(5):1009–1021
28. Farashi S, Vafaee F (2022) Effect of extruder temperature and printing speed on the tensile strength of fused deposition modeling (FDM) 3D printed samples: a meta-analysis study. Int J Interac Des Manuf 16(1):305–316
29. Sharon JA, Padilla HA, Boyce BL (2013) Interpreting the ductility of nanocrystalline metals1. J Mater Res 28(12):1539–1552
30. Sheoran AJ, Kumar H (2020) Fused Deposition modeling process parameters optimization and effect on mechanical properties and part quality: review and reflection on present research. Mater Today 21:1659–1672
31. Morettini G, Palmieri M, Capponi L et al (2022) Comprehensive characterization of mechanical and physical properties of PLA structures printed by FFF-3D-printing process in different directions. Prog Addit Manuf 7(5):1111–1122
32. Bootsma K, Fitzgerald MM, Free B et al (2017) 3D printing of an interpenetrating network hydrogel material with tunable viscoelastic properties. J Mech Behav Biomed Mater 70:84–94
33. Costanzo A, Spotorno R, Candal MV et al (2020) Residual alignment and its effect on weld strength in material-extrusion 3D-printing of polylactic acid. Addit Manuf 36:101415